Journal Pre-proofs

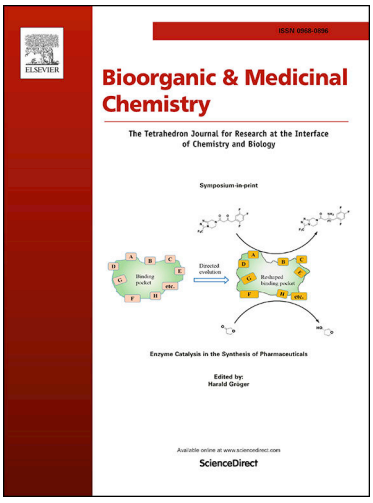

Identification of *Mycobacterium tuberculosis* CtpF as a target for designing new antituberculous compounds

Paola Santos, Fabian Lopez-Vallejo, David Ramírez, Julio Caballero, Dulce Mata Espinosa, Rogelio Hernández-Pando, Carlos Y. Soto

PII: S0968-0896(19)31799-7
DOI: https://doi.org/10.1016/j.bmc.2019.115256
Reference: BMC 115256

To appear in: *Bioorganic & Medicinal Chemistry*

Received Date: 22 October 2019
Revised Date: 4 December 2019
Accepted Date: 6 December 2019

Please cite this article as: P. Santos, F. Lopez-Vallejo, D. Ramírez, J. Caballero, D. Mata Espinosa, R. Hernández-Pando, C.Y. Soto, Identification of *Mycobacterium tuberculosis* CtpF as a target for designing new antituberculous compounds, *Bioorganic & Medicinal Chemistry* (2019), doi: https://doi.org/10.1016/j.bmc.2019.115256

Identification of *Mycobacterium tuberculosis* CtpF as a target for designing new antituberculous compounds

Paola Santos[a], Fabian Lopez-Vallejo[a]*, David Ramírez[b], Julio Caballero[c], Dulce Mata Espinosa[d], Rogelio Hernández-Pando[d] and Carlos Y. Soto[a]

[a] Departamento de Química, Facultad de Ciencias, Universidad Nacional de Colombia, Carrera 30 N° 45-03, Bogotá, Colombia.

[b] Instituto de Ciencias Biomédicas, Facultad de Ciencias de la Salud, Universidad Autónoma de Chile, El Llano Subercaseaux 2801- Piso 5, 8900000 Santiago, Chile.

[c] Centro de Bioinformática y Simulación Molecular, Universidad de Talca, 2 Norte 685, Casilla 721, Talca, Chile.

[d] Unidad de Patología Experimental, Departamento de Patología, Instituto Nacional de Ciencias Médicas y Nutrición Salvador Zubirán, Vasco de Quiroga 15, Belisario Domínguez Secc 16, 14080, México City, México

*Corresponding author: Departamento de Química, Facultad de Ciencias, Universidad Nacional de Colombia, Carrera 30 N° 45-03, Ciudad Universitaria, Bogotá, Colombia; Oficina: 415; Tel: 57-1-3165000 / Ext: 14445; Fax: 57-1-3155220; e-mail: fhlopezv@unal.edu.co

Abstract

The emergence of tuberculosis (TB) produced by multi-drug resistance (MDR) and extensively-drug resistance (XDR) *Mycobacterium tuberculosis* (*Mtb*), encourages the development of new antituberculous compounds, as well as the identification of novel drug targets. In this regard, plasma membrane P-type ATPases are interesting targets because they play a crucial role in ion homeostasis and mycobacterial survival. We focused on *Mtb* CtpF, a calcium P-type ATPase that responds to a broad number of intraphagosomal conditions, as a novel target. In this study, we evaluated the capacity of cyclopiazonic acid (CPA), a well-known inhibitor of the sarco-endoplasmic reticulum Ca^{2+}-ATPase (SERCA), to inhibit the ATPase activity of CtpF and the *Mtb* growth demonstrating that CtpF is a druggable target. A homology modeling of CtpF was generated for molecular docking studies of CtpF with CPA and key pharmacophoric features were identified, which were used to perform a pharmacophore-based virtual screening of the ZINC database, and to identify CtpF inhibitor candidates. Molecular docking-based virtual screening and MM-BGSA calculations of candidates allowed identifying six compounds with the best binding energies. The compounds displayed *in vitro* minimum inhibitory concentrations (MIC) ranging from 50 to 100 μg/mL, growth inhibitions from 29.5 to 64.0% on *Mtb*, and inhibitions of Ca^{2+}-dependent ATPase activity in *Mtb* membrane vesicles (IC_{50}) ranging from 4.1 to 35.8 μM. The compound ZINC63908257 was the best candidate by displaying a MIC of 50 μg/mL and a Ca^{2+} P-type ATPase inhibition of 45% with IC_{50} = 4.4 μM. Overall, the results indicate that CtpF is a druggable target for designing new antituberculous compounds.

Keywords: Tuberculosis; Antimycobacterial therapeutics; Cyclopiazonic acid; P-type ATPases, Molecular docking.

1. Introduction

Tuberculosis (TB) remains as one of the most relevant public health problems worldwide. In 2017, there were at least 1.3 million deaths by TB [1]. This health problem has been exacerbated by latent infections and the high prevalence of human immunodeficiency virus (HIV)-TB coinfection [2]. The long lasting anti-TB treatment is due in part to the difficulty of achieving therapeutic concentrations of antituberculous drugs inside mycobacterial cells, which is partly caused by the low permeability of the mycobacterial cell wall, and the limited effects of drugs against latent infections [2]. The capacity of *Mycobacterium tuberculosis* (*Mtb*) to rapidly generate drug resistance raises the need for discovering alternative TB targets and new compounds to be administered in combination with the traditional anti-TB drugs.

Plasma membrane proteins are advantageous as drug targets because potential antimicrobial compounds do not need to cross the cell envelope [3]. In this context, different anti-TB drugs such as bedaquiline, have been developed. This drug interferes with proton pumping and ATP synthesis mediated by the F_1F_0-ATPase in the mycobacterial plasma membrane [4]. Similarly, SQ109 blocks the trehalose mono-mycolate transporter MMPL3 that is essential for mycolic acid biosynthesis in mycobacteria [5].

On the other hand, recent studies highlight the importance of mycobacterial plasma membrane P-type ATPases in the ionic homeostasis of heavy metal cations and bacterial intrafagosomal survival [6]. P-type ATPases have been the target of successful antimicrobial compounds; for instance, of antimalarial artemisinin, which inhibits PfATP6, a sarco-endoplasmic reticulum Ca^{2+}-ATPase (SERCA)-type of *Plasmodium falciparum* [7]. From this point of view, P-type ATPases are interesting targets for designing new anti-TB drugs.

P-type ATPases contain three cytoplasmic domains: nucleotide binding (N), phosphorylating (P), and actuator (A); together with two transmembrane domains (TMDs), namely transmembrane transport (T) and class-specific support domains (S) [8]. In addition, P-type ATPases have two conformational states: E1, in which ions are attached to the cytoplasmic side of the cell membrane to promote autophosphorylation, generating a new conformational state, and E2 state, in which the substrate has a

low affinity, promoting ion translocation across the cell membrane [9]. Although P-type ATPases share a catalytic mechanism based on the conformational changes of the five structural domains, the regulatory mechanisms and ion affinity differ among them.

The *Mtb* genome contains 11 P-type ATPases, which are classified according to the type of transported cations as follows: *i)* heavy-metal transporters, which include CtpA, CtpB, CtpC, CtpD, CtpG, CtpJ and CtpV, and *ii)* alkali / alkaline earth transporters, including CtpE, CtpF, CtpH, and CtpI [10]. Several *Mtb* P-type ATPases display relevant biological functions; e.g. CtpV is involved in Cu^{2+} tolerance [11], CtpC is associated with Zn^{2+} efflux [12], and CtpD shows affinity for both Co^{2+} and Zn^{2+}, suggesting that P-type ATPases can be multifunctional enzymes. In experimental conditions mimicking latent infections, mycobacteria down-regulate ATPases except for those that are essential for ATPase activity in ATP scarcity, such as Na^{+}/K^{+} and Ca^{2+} transporters [13].

Mtb CtpF (Rv1997) is a putative Ca^{2+} transporter, which is activated in response to stress conditions associated with infection [14]. Thus, CtpF is involved in the mycobacterial response to oxidative stress, which is faced by intracellular pathogens during the infection process. CtpF is the mycobacterial P-type ATPase closest to eukaryotic SERCA1a isoform (35.3% sequence identity), the most extensively studied P-type ATPase [15]. A specific and potent inhibitor of SERCA is cyclopiazonic acid (CPA), a toxic tetramic indole acid naturally produced by the fungi *Penicillium* and *Aspergillus*. CPA acts on the transmembrane segments (TMDs) involved in calcium transport by P-type ATPases, making them rigid and blocking Ca^{2+} transport [16].

In this study, a model of CtpF was constructed by homology modeling using SERCA1a co-crystallized with CPA as a template. The most important interactions between CtpF and CPA were predicted using molecular docking calculations, and a CtpF-ligand pharmacophoric pattern was proposed. This information was used for a screening of the ZINC database. Thereafter, docking studies of the pharmacophore-based top candidates and MM-GBSA re-scoring allowed identifying six compounds with high binding energies. For these compounds, we estimated inhibition of the Ca^{2+}-dependent P-type ATPase activity and antimycobacterial activity *in vitro*. We found that ZINC63908257 was the most

active compound without causing high toxicity in eukaryotic cells.

2. Results and discussion

2.1 Homology modeling of CtpF

To date, there are no crystallographic structures of *Mtb* P-type ATPases. Analysis of amino acid sequence, reflects that CtpF-*Mtb* is an alkaline/alkaline earth cation transporter with homology to eukaryotic SERCA1a isoform [17]; therefore, the three-dimensional (3D) structure of CtpF-*Mtb* was predicted by homology modeling by using the crystal structure of SERCA1a in an E2.P-like form and stabilized with cyclopiazonic acid (CPA), as template. Both amino acid sequences show 35.3% of identity according to Clustal Omega tool [18] (Supplementary Material, Fig. S1).

The model CtpF-*Mtb* was stabilized in a realistic biological media and its conformational sampling was obtained by performing a 20-ns molecular dynamics simulation; the most stable conformation of this simulation was selected to have a more reliable model of CtpF. Similar to SERCA and other P-type ATPases [8], the CtpF model consists of three cytoplasmic domains; a nucleotide binding domain (N) connected to a phosphorylation domain (P), an actuator domain (A), and ten transmembrane helices (TMDs), M1 to M10 (Figure 1A). The stereochemical quality of CtpF was assessed with PROCHECK and the results revealed that 91% of the residues are in the most favorable regions of the Ramachandran plot and the root mean square deviation (RMSD) to the SERCA1a template is 0.890 Å, proving that the our CtpF model is accurate and reliable (Figure 1B). Additionally, the model was validated using ProSA-web, which measured the deviation of the total energy of the structure compared to an energy distribution derived from random conformations. The analysis yielded a z-score of -5.98, indicating a good overall quality (Figure 1C). Both SERCA1a and CtpF 3D structures showed very similar global structure, including the majority of residues around the CPA binding site with nearly identical positions. Taking the quality information above, we considered that our CtpF model has enough quality for structure-based

drug design purposes.

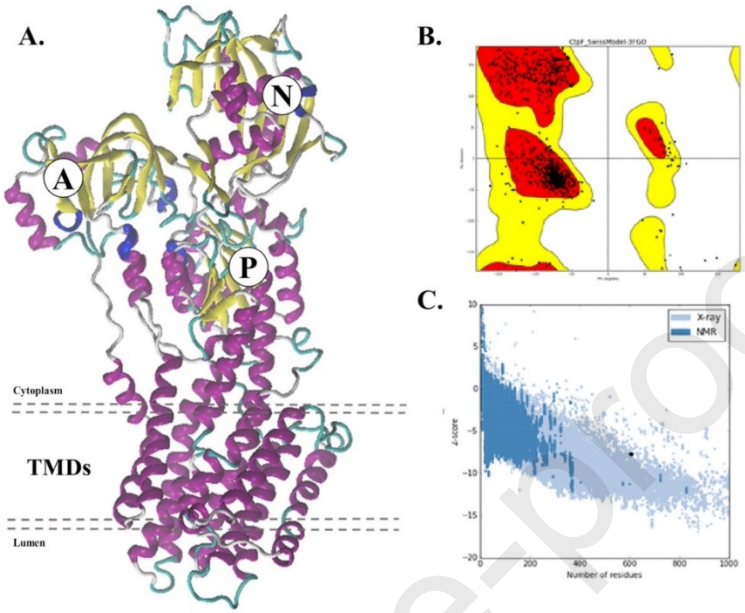

Figure 1. CtpF 3D structure and validation. **A.** CtpF structural model predicted by homology modeling: the cytoplasmic domains are represented: (N) the nucleotide-binding, (P) phosphorylation, (A) actuator and transmembrane domains (TMDs). **B.** Ramachandran plot. **C.** ProSA plot: the z-score of CtpF is highlighted with a black dot.

2.2 Molecular docking of CPA with the CtpF model and SERCA1a

Docking of CPA inside the CtpF model was compared with the same ligand inside SERCA1a. As a result, the obtained pose was in agreement with the binding mode of SERCA1a-CPA crystal structure PDB code: 3FGO [19]. Figure 2 shows the alignment of SERCA1a and the CtpF model after CPA docking calculations. The similarity between the binding mode of CPA inside both proteins indicate that this ligand should have the same orientation in both highly conserved binding sites.

According to previous crystallographic structure reports, the CPA binding site is formed by two pockets; a polar one oriented towards M1 and M2 (with residues Gln56 and Asn101 of SERCA1a) where short

contacts with the tetramic acid moiety of CPA are established. In this polar region, there are reports of additional interactions with Gln56 mediated by a water molecule [20], and other authors have described that a divalent metal ion is required for CPA binding through the coordination of the tetramic acid moiety [19]. The other CPA union pocket is hydrophobic and adjacent to M3 and M4, making short contacts with the indole ring.

The self-docking of CPA inside SERCA1a led to the same orientation, with an RMSD values of 0.325 Å. Docking of CPA inside CtpF led also to the same orientation with an RMSD value of 0.665 Å (Figure 2).

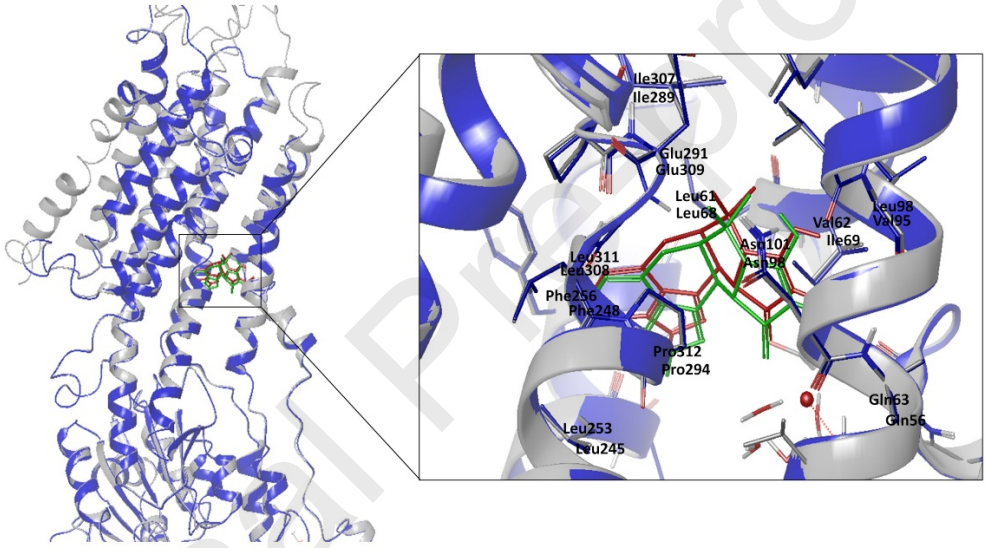

Figure 2. Molecular docking results of CPA inside SERCA1a and CtpF. Structural alignment of 3FGO (gray) and the CtpF model (blue), with CPA inside SERCA1a (self-docking: green) and inside CtpF (red). The residues that represent the most important interactions within 4 Å are shown.

Table 1 represents the residues in the surrounding (4 Å) of CPA in both SERCA1a and CtpF binding sites. Among the 13 identified residues, the main differences between the two sequences lies in Asp59, Val62, and Leu98 in SERCA1a that correspond in sequence to His66, Ile69 and Val95 respectively in

CtpF. All these residues are close to the tetramic acid moiety of CPA.

Table 1. Comparison of the CPA binding site residues for SERCA1a and CtpF (residues within 4.0 Å from CPA). The residues that are different in the two proteins are shown in bold letters

Binding site residues of SERCA1a	Binding site residues of CtpF
Gln56	Gln63
Asp59	**His66**
Leu61	Leu68
Val62	**Ile69**
Leu98	**Val95**
Asn101	Asn98
Ala102	Ala99
Leu253	Leu245
Phe256	Phe248
Ile307	Ile289
Glu309	Glu291
Leu311	Leu308
Pro312	Pro294

2.3 Virtual screening and identification of theoretical candidates

CtpF-CPA molecular docking was used to construct a hypothetical pharmacophore model derived from the main interactions identified between CPA and its receptor. The next step was to identify the features to be considered as part of this pharmacophore. The selected pharmacophoric model was formed by two hydrogen bond (H-bond) donors (D1 and D2), two H-bond acceptors (A1 and A2), and a hydrophobic group (H1) (Figure 3). Using this model, a pharmacophore-based virtual screening (PBVS) was performed with the ZINCPharmer online interface (http://zincpharmer.csb.pitt.edu) and the purchasable

ZINC database with 22,723.923 compounds. The PBVS brought 362 candidates, which were later subjected to a docking-based virtual screening (DBVS) with Glide SP and XP methods.

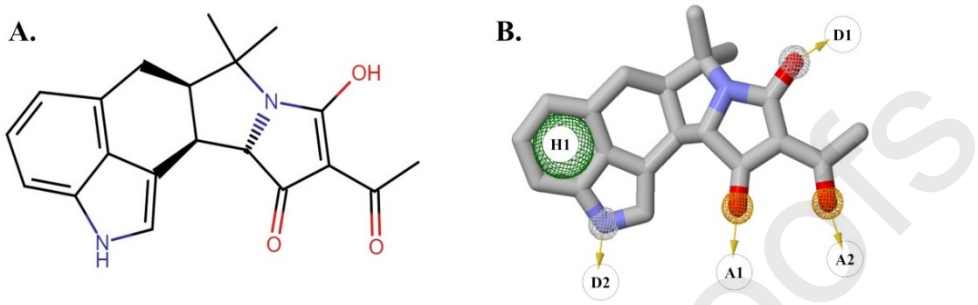

Figure 3. Pharmacophore model. **A.** Structural features of CPA **B.** CPA pharmacophoric features D1, D2, A1, A2, and H1.

It is well known that docking scoring is not reliable because it does not consider main factors such as solvent terms of the binding energy. Therefore, Molecular Mechanics/Generalized Born Surface Area (MM/GBSA) re-scoring was applied to the top one hundred compounds obtained after Glide XP docking in order to rescore the DBVS results. MM/GBSA was used to model solvent effects by continuum solvation and a surface area dependent terms; it is well known that such approximation is more reliable to predict free energy differences between compounds identified with docking [21]. This type of approach has been applied successfully to the study of interactions between series of compounds with multiple molecular targets [22].

Six compounds were identified among the ones with the best MM-GBSA re-scoring energies and they were selected from the full list, and afterwards purchased for experimental evaluations. Several considerations were taken into account for selection of the best compounds, i.e. high binding free energies, scaffold diversity, drug-like properties, and cost. The selected compounds, shown in Table 2, displayed better MM-GBSA binding energies than CPA (-47.09 kcal/mol) and ranged from -49.62 to -70.13 kcal/mol.

Table 2. CPA and candidate compounds selected by applying virtual screening to ZINC database. Drug-like properties and binding free energies from molecular docking and ΔG MM-GBSA

Compound	Structure	MW	LogP	H-bond donors	H-bond acceptors	tPSA	RB	Glide Score*	ΔG MM – GBSA*
Cyclopiazonic acid (CPA)	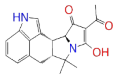	336.4	2.21	2	3	73	1	- 47.09	-7.57
ZINC63908257	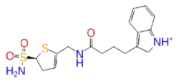	377.5	1.68	4	6	103	7	-59.28	-8.26
ZINC55090623	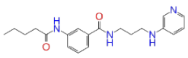	354.4	2.91	3	6	83	10	-59.04	-8.04
ZINC45605493	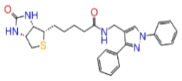	475.6	3.34	3	7	88	9	-70.13	-7.68
ZINC14541509		434.5	3.32	3	9	115	11	-57.59	-7.07
ZINC09787234	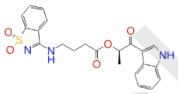	439.4	1.82	2	8	117	9	-66.42	-6.92
ZINC12584082	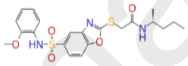	463.5	4.08	2	8	111	10	-49.62	-5.92

Drug-like properties: molecular weight (MW), octanol-water partition coefficient log (LogP), number of hydrogen bond donors (H-bond donors); number of hydrogen bond acceptors (H-bond acceptors); topological polar surface area (tPSA); number of rotatable bonds (RB). **Glide score and ΔG MM-GBSA** calculations *energy in: kcal / mol.

2.4 Biological activity of the candidate compounds

CPA and the six select compounds from the MDVS + MM-GBSA protocol were tested for their antimycobacterial activity against the standard *Mtb* H37Rv strain (Table 3). The MIC test using resazurin

as viability indicator showed that almost all tested compounds, except ZINC12584082, inhibit mycobacterial growth. The MIC displayed by ZINC63908257 and ZINC14541509 was 50 µg/mL, which was 0.5-fold lower than the value showed by CPA and the other compounds assessed.

Table 3. Bioactivity results of CPA and six compounds selected by virtual screening from the ZINC database. The % of growth inhibition, cytotoxicity and hemolysis were estimated by supplementing the assays with 100 µg/mL of the selected compounds and CPA. The enzymatic activity represents the effect of the compounds on the Ca^{2+}-ATPase activity. All evaluations were obtained from three independent experiments

	Antimycobacterial activity		Safety evaluation (at 100 µg/ml)		Enzymatic activity IC_{50} (µM) ± SEM	
Compound	MIC (µg/mL)	Inhibition (%)	Cytotoxicity (%)	Hemolytic activity (%)	*Mtb* WT	*Mtb* Δ*ctpF*
Cyclopiazonic acid (CPA)	100	29.9	50.8	6.6	7.2 ± 0.3	94.5 ± 1.2
ZINC63908257	50	64.0	12.9	2.0	4.4 ± 0.3	100.5 ± 1.9
ZINC55090623	100	52.9	21.4	1.2	4.2 ± 0.2	96.9 ± 2.4
ZINC45605493	100	29.5	30.0	2.4	4.1 ± 0.2	76.1 ± 1.9
ZINC14541509	50	60.7	19.8	0.6	8.0 ± 0.6	38.4 ± 1.1
ZINC09787234	100	37.3	31.6	2.1	11.8 ± 0.6	101.9 ± 1.6
ZINC12584082	> 200	N/A	39.5	1.0	35.9 ± 0.5	109.4 ± 2.3

The compounds ZINC63908257 and ZINC14541509 showed mycobacterial growth inhibitions of 64.0% and 60.7%, respectively. Since an antimycobacterial compounds must cross the wide and complex cell wall, percentages of *Mtb* growth inhibition higher than 60% suggest can be considered as significant antimycobacterial activity. Regarding the hydrophobicity of the compounds, current anti-TB drugs have a low LogP, meaning that they are hydrophilic [23]. The most active compound, ZINC63908257, showed a low LogP = 1.68 compared with less active ZINC12584082, which had the highest LogP = 4.08 (Table 2). This suggests that active compounds might follow a pathway different from passive diffusion to cross

the mycobacterial cell envelope to reach the CtpF target.

The hemolytic and cytotoxic activities were quantified to estimate the potentially harmful action of the compounds on eukaryotic cells (Table 3). All the selected compounds showed cytotoxic activity with values lower than 40%. Interestingly, the most active compounds against mycobacterial cells, namely ZINC63908257 and ZINC14541509, showed the lowest cytotoxic activities on the MH-S cell line of murine macrophages (12.9% and 19.8%, respectively). Meanwhile, CPA displayed cytotoxicity with a value of 50.8%, as observed in previous reports for this reference substance [24]. Regarding the hemolytic activity, none of the compounds tested at 100 µg/mL showed activity greater than 2.5% compared to the positive controls. In contrast, CPA showed hemolysis of 6.6% at 100 µg/mL. In conclusion, we highlight the safety of ZINC63908257, which displayed the highest antimycobacterial activity and lowest toxicity in eukaryotic cells; thus, this compound shows a good pharmacokinetic profile (drug-like).

2.6 Effect of CPA and the selected compounds on Ca^{2+}-ATPase activity

The selected compounds were subsequently assessed for their capacity to inhibit the Ca^{2+}-ATPase activity of the *Mtb* H37Ra plasma membrane compared to CPA, a well-known inhibitor of the Ca^{2+}-ATPase activity in SERCA [25]. As a starting point, we determined the basal ATPase activity (in the absence of Ca^{2+}), the Ca^{2+}-dependent ATPase activity (in the presence of calcium), and the specific P-type ATPase activity in the presence of vanadate, an inhibitor of P-type ATPases [26], in membrane vesicles obtained from *Mtb* H37Ra wild type (*Mtb* WT) and *Mtb* H37Ra cells defective in *ctpF* (*MtbΔctpF*) as control. Thus, the specific Ca^{2+} P-type ATPase activity was estimated as the difference between the Ca^{2+}-dependent ATPase activity and the Ca^{2+} ATPase activity in the presence of vanadate (50 µM). We found that Ca^{2+} (30 µM) activated the basal ATPase activity of *Mtb* WT by 30%, whereas the enzyme activity of the membrane vesicles obtained from *MtbΔctpF* cells was activated by approximately 7% (Figure 4A). These differences indicate that there is Ca^{2+}-P-type ATPase activity in the *Mtb* plasma membrane mediated by CtpF.

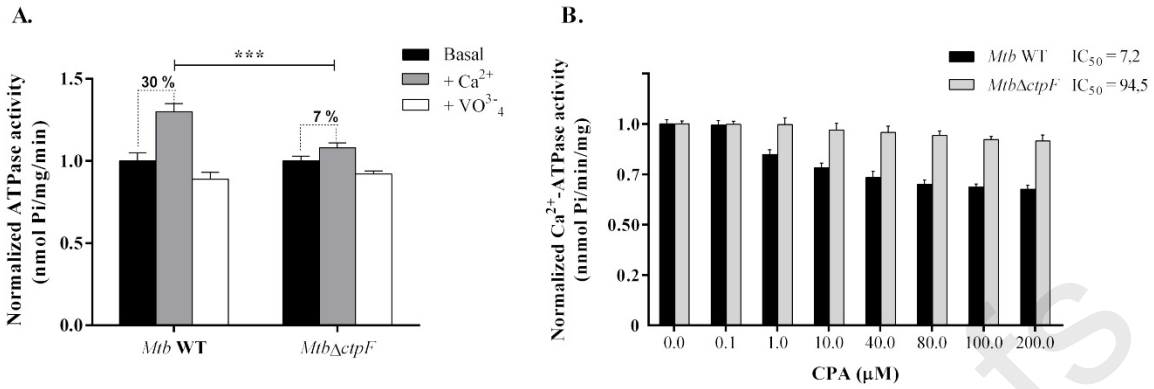

Figure 4. Inhibitory effect of CPA on Ca^{2+}-ATPase activity. **A.** Determination of basal and Ca^{2+}-dependent ATPase activity in membranes from *Mtb* WT and *MtbΔctpF* cells. The Ca^{2+}-ATPase activity was measured by the addition of Ca^{2+}-free (30 µM). Values are compared with the activity obtained in the presence of vanadate (VO^{3-}_4 = 50 µM). Values are the means ± SEM (n = 3). Significant differences observed between strains are marked by asterisks as ***, $P < 0.001$. **B.** The effect of CPA (0.1, 1, 10, 40, 80, 100 and 200 µM) on the normalized Ca^{2+}-ATPase activities of *Mtb* WT and *MtbΔctpF* is indicated; the results were expressed as means ± SEM (n = 3) of the Ca^{2+}-ATPase activity. The IC_{50} was calculated by non-linear regression using GraphPad Prism software package 5.04.

We also assessed the effect of CPA on the Ca^{2+}-ATPase activity in the *Mtb* plasma membrane (Figure 4B). CPA considerably inhibited the enzymatic activity in *Mtb* WT cells in a concentration-dependent manner (from 1.0 µM, with $IC_{50} = 7.2 \pm 0.3$ µM) compared with the enzymatic activity displayed by the *MtbΔctpF* cells. In this way, our results reveal that CPA inhibits mycobacterial Ca^{2+}-ATPase activity mediated by CtpF at concentrations comparable to those reported for SERCA1a and PfATP6 [27].

Little is known about the intracellular regulation systems of Ca^{2+} in bacteria. Previous reports indicate that *Listeria monocytogenes* Ca^{2+}-ATPase (LMCA1) and SERCA1a share a high sequence similarity (38%), and that the CPA binding pocket in both proteins differs by only four amino acids [28]. These amino acid residues are important for the coordination of CPA and partly explain why LMCA1 is inhibited at very high CPA concentrations (918 ± 38 µM). In addition, putative Ca^{2+} -ATPases homologous to SERCA1a have been identified in other bacterial genomes, such as *Lactobacillus lactis* (LLCA1), *Bacillus cereus* (BACCA1) and *Streptococcus pneumoniae* (CaxP). The Ca^{2+} -ATPase activity mediated

by CaxP is key for bacterial survival at high concentrations of extracellular Ca^{2+} inside macrophages [29]. Despite the high identity of these proteins with SERCA1a, only BACCA1 retains the same coordination residues with CPA displayed by SERCA1a, thus, BACCA1 is sensitive to CPA showing an IC_{50} of 4 µM [28]. On the other hand, CPA also induces an increase of the intracellular concentration of Ca^{2+} of the respiratory syncytial virus (RSV), altering the viral replication and transcription and therefore showing antiviral activity [30].

In our case, CPA inhibits CtpF with an IC_{50} value in the same range as SERCA1a (CPA-sensitive P-type ATPase). Therefore, CtpF behaves similarly to SERCA1a as compared with other Ca^{2+}-ATPases that are inhibited at high CPA concentrations.

On the other hand, all the six selected compounds inhibited the Ca^{2+}-ATPase activity in the cell membrane of *Mtb* WT, as shown by the IC_{50} values in Table 3. Since there is not Ca^{2+}-ATPase activity mediated by CtpF in *MtbΔctpF*, as expected, the selected compounds did not alter the enzymatic activity in the cell membrane of mutant cells.

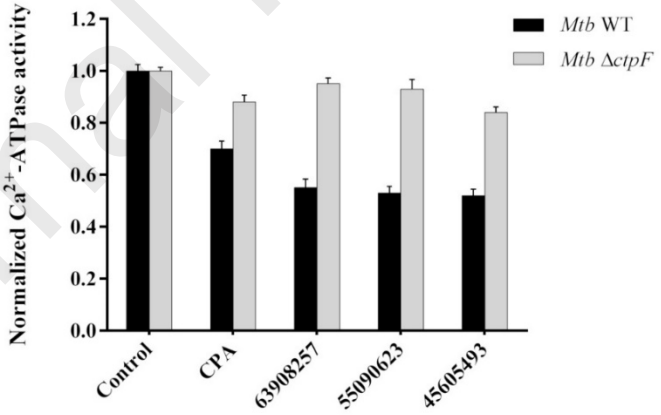

Figure 5. Effect of CPA and the selected compounds on the normalized Ca^{2+}-ATPase activity of *Mtb* WT and *MtbΔctpF* cell membranes. The activity is shown at a concentration of 100 µM. Mean values ± SEM (n = 3) are shown.

As shown in Figure 5, the three compounds with the highest activity: ZINC63908257, ZINC55090623,

and ZINC45605493 (at 100 μM) inhibited the Ca^{2+}-ATPase activity in *Mtb* WT cell membranes by 44.9%, 46.9% and 48.2%, respectively, compared with the inhibition of the Ca^{2+}-ATPase activity observed in membranes obtained from mutant cells (*MtbΔ*ctpF). Finally, among the six selected compounds, ZINC63908257 was the highest inhibitor of the Ca^{2+}-ATPase activity (IC_{50} = 4.4 ± 0.3 μM) and the bacterial cell viability (64%) of *Mtb* H37Rv cells. These results strongly suggest a correlation between the inhibition of Ca^{2+}-ATPase activity of the plasma membrane, and mycobacterial viability. Therefore, ZINC63908257 could be further developed into a drug candidate by a medicinal chemistry approach.

2.7 Protein binding site and bioactivity analysis

Taking together docking and the bioactivity profiles (MIC, % growth inhibition, and inhibition of Ca^{2+}-ATPase activity) of the six selected compounds, we highlight three compounds with superior bioactivity profiles: ZINC63908257, ZINC55090623, and ZINC45605493, as displayed in Table 3. The tested compounds showed not only better IC_{50} values than CPA, ranging from 4.1 to 4.4 μM, but also higher mycobacterial growth inhibitions.

Figure 6 shows the binding modes for CPA and the three most active compounds into the pocket formed by the TMDs segments M1 - M4 of CtpF by using docking. Since the surface areas of these three compounds are bigger than that of CPA (Figure 6A), we expected these to occupy the calcium access channel and, an extended binding site (toward a more polar region of the TMDs segments M1, M2 and M4). It is noteworthy to mention that this groove is an unexplored binding pocket that does not make short contacts with CPA. All short contacts between CtpF and the most relevant compounds (CPA and the three most active compounds) are summarized in Table 4. For instance, ZINC63908257 makes short contacts with M1 residues (Gln63, His66, and Ile69); M2 (Gly102, Gln105, and Glu106), and M3 (Thr242, Leu245, and Ala246), occupying the calcium access channel. This compound, with an LogP value of 1.68, is slightly more hydrophilic than CPA, more active (IC_{50} of 4.4 μM), and has growth inhibition of 64.0% (Figure 6B). The imidazolone ring of ZINC45605493 orients mainly towards the

cytoplasmic region of the calcium access channel, making short contacts with more hydrophilic residues of the TMDs segments M1 (Arg62), M2 (Glu106) and forms a H-bond with Arg317 from a random coil next to segment M3. This compound also makes short contacts with more hydrophilic residues of TMDs segments M1 (Arg62), M2 (Glu106), and form an H-bond with Arg317 from a random coil next to the segment M3. This compound also makes short contacts with residues of the segments M1 - M4 that form the CPA binding pocket (Figure 6D). Finally, compound ZINC45605493 displays the best IC_{50} (4.1 μM) and, shows the lowest percentage of growth inhibition (29.5%). The LogP value (3.34) suggests that a lower LogP value should be needed to improve the percentage of growth inhibition (as in the case of ZINC63908257).

Although ZINC55090623 (Figure 6C) is a longer than CPA, it folds to bind in a similar way as CPA and interacts mainly with the residues of segments M1 (Gln63, His66, Leu68, Ile69), M2 (Val95, Asn98, Ala99, and Gly102), M3 (Leu245, Ala246, Phe248, and Ser249), and M4 (Ile289, Glu291, Pro290, Leu293, and Pro294). It exhibits an H-bond with Pro290 as ZINC63908257, but does not make short contacts towards the cytoplasmic polar region as ZINC63908257, and ZINC45605493. ZINC55090623 displays an important IC_{50} of 4.2 μM, a percentage of growth inhibition of 52.9%, and a LogP value of 2.91.

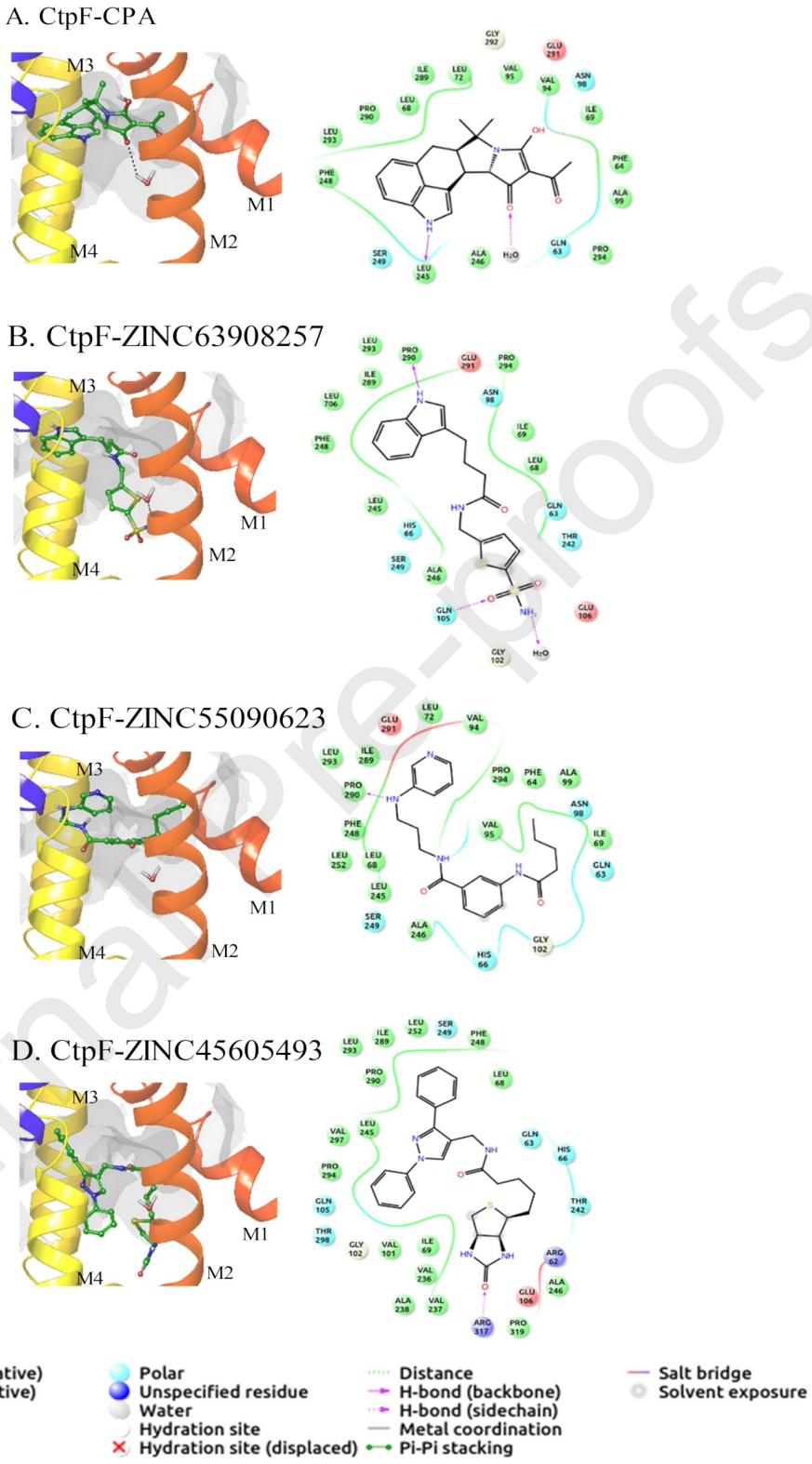

Figure 6. 3D and 2D binding modes of CPA and the most active inhibitors with CtpF model. **A.** CPA; **B.**

ZINC63908257; **C.** ZINC55090623 and **D**. ZINC45605493. All residues shown are at 4 Å from ligand.

In order to quantitatively calculate the binding mode similarity between the three most active compounds (ZINC63908257, ZINC55090623, and ZINC45605493) and CPA as reference, protein-ligand interaction fingerprint (PLIF) values were determined (Table 4). ZINC63908257 shows the most similar binding mode to CPA, with 88.2% of similarity (Tanimoto coefficient = 0.88). This compound shares similar residues that compose the CPA binding site. On the contrary, ZINC45605493, with the highest IC_{50} value, has the lowest Tanimoto similarity, with, 0.33 or 33.3%. This can be explained by the interactions with residues located towards the cytoplasmic region of the calcium access channel. These results suggest that it is important to explore pockets at the cytoplasm border, in order to identify more potent anti-ATPase inhibitors.

Table 4. Binding site residues (TMDS segments M1 - M4) for CPA and the most active compounds. All residues are at a maximum of 4 Å from the ligands. Tanimoto similarity binding mode

Compound	Residues at 4Å from ligands	Tanimoto similarity
CPA	**M1** (Gln63, Leu 68, Ile69, Leu72); **M2** (Val95, Asn98, Ala99, Gly102); **M3** (Leu245, Phe248, Ser 249); **M4** (Ile289, Pro290, Leu293, Pro294)	1.00
ZINC63908257	**M1** (Gln63, Hys66, Leu68, Ile69); **M2** (Asn98, Ala99, Gly102, Gln105, Glu106); **M3** (Thr242, Leu245, Ala246, Phe248, Ser 249); **M4** (Ile289, Pro290, Glu291, Leu293, Pro294)	0.88
ZINC55090623	**M1** (Gln63, Hys66, Leu68, Ile69, Leu72); **M2** (Val95, Asn98, Ala99, Gly102); **M3** (Leu245, Ala246, Phe248, Ser 249); **M4** (Ile289, Pro290, Glu291, Leu293, Pro294)	0.38
ZINC45605493	**M1** (Gln63, Hys66, Leu68, Ile69); **M2** (Ala99, Val101, Gly102, Gln105, Glu106); **M3** (Thr242, Leu245, Ala246, Phe248, Ser 249, Leu252); **M4** (Ile289, Pro290, Pro294, Val297)	0.33

A similar study using the SERCA ortholog PfATP6 of *Plasmodium falciparum*, showed that PfATP6 is highly inhibited by CPA, suggesting that the molecular mechanism of CPA and the binding site is conserved for both proteins [27]. Additionally, studies with PfATP6 expressed in *Xenopus* oocytes, as well as mutagenesis, biochemical assays, and molecular modelling techniques, have suggested PfATP6 as the target of antimalarial artemisinin [31]. Other studies have indicated that the artemisinin binding pocket in PfATP6 is close to the thapsigargin and CPA pocket in SERCA1a, thus, affecting calcium transport in a similar way [32]. Consistent with these findings, CPA sensitive Ca^{2+}-ATPases such as CtpF, could likewise be a target for the development of antituberculous drugs.

Conclusions

Our results indicate that CtpF is a CPA-sensitive P-type ATPase associated with Ca^{2+} transport in *Mtb* cells. For the first time, a molecular modeling-based approach was used to successfully identify novel CtpF inhibitors. We highlight ZINC63908257, as lead compound, which disrupts the CtpF enzymatic activity and displays inhibition of *Mtb* H37Rv growth. These results suggest a connection between the Ca^{2+}-ATPase activity and mycobacterial survival, showing CtpF as a druggable target.

In addition, future research to optimize the potency of compounds against *Mtb* will be a priority. A new strategy to design anti-TB compounds by, targeting CtpF, will require molecules with an intermediate polarity (LogP around 2.0) that make more short contacts to the polar region formed by TM1, TM2 and TM4, which is an unexplored groove. Overall, our results suggest that structure-based pharmacophore modeling provides useful information for a proper understanding of the structural and binding features relevant for designing novel P-type ATPase inhibitors as antituberculous compounds.

4. Experimental section

4.1 Computational studies

4.1.1 Modeling of CtpF

The CtpF-*Mtb* 3D structure was obtained by homology modeling by using the energy-based method on the web server Swiss-Model [33]. The query sequence of CtpF-*Mtb* (UniProt ID: P9WPS9) was retrieved from the UniProtKB protein database. An available crystallographic structure of SERCA1a in an E2.P state with bound CPA (PDB code 3FGO) [19] was used as template. This template was selected after studying eight structures of SERCA1a-CPA complexes available in the PDB, with acceptable resolution (2.4 Å) (Supplementary Material, Fig. S2). The selected template displays a divalent metal (Mn^{2+}) and three water molecules in the CPA binding site. Nevertheless, the CtpF homology model was built keeping one water molecule present in the CPA active site instead of Mn^{2+} since the reported crystallographic structures show a conserved water molecule that is important for CPA binding [20].

In order to relax the CtpF model, a 20-ns restrained molecular dynamics (MD) simulation, using Desmond v.2.3 software and the OPLS_2005 force field [34], was carried out. For this, the CtpF model was inserted in a 1-palmitoyl-2-oleoyl-phosphatidylcholine (POPC) membrane, solvated into an orthorhombic box with a buffer distance of 10 Å. The model was neutralized by adding 12 Na^+ ions to balance the net charge of the systems and $MgCl_2$ was introduced at a concentration of 2.5 mM. The entire system was first minimized and, then equilibrated with the default relaxation process of six stages for the NPT ensemble. Desmond simulation parameters were kept to their default values for the 20-ns MD production run: ensemble NPT, constant temperature at 300^o K using the Nosé-Hoover chain thermostat, and constant pressure at 1 atm using the Martyna-Tobias-Klein barostat, with relaxation times of 1 and 2 ps, respectively. Finally, ProSa. Finally, ProSA-web [35] and PROCHECK [36] programs were used to assess the quality of the resulting molecular structure.

4.1.2 Dataset preparation

The 3D structures of CPA and the candidates resulting from the virtual screening (downloaded from the ZINC database) [37] were curated and prepared with LigPrep module (LigPrep, Schrödinger, LLC, New York, NY, 2016), where ionization states were generated at pH 7.0 ± 2.0 using Epik. Energy minimization was performed during each ligand preparation using Macromodel [38] with the OPLS_2005 force field. The drug-like properties for each ligand such as molecular weight (MW), octanol-water partition coefficient log (LogP), number of H-bond donors, number of H-bond acceptors, topological polar surface area (tPSA), and number of rotatable bonds (RB), were also calculated with Maestro.

4.1.3 Molecular docking

To ensure that the docking methodology could reproduce the crystal conformation, a reconstruction of the ligand-receptor complex by performing docking of CPA in its own SERCA1a crystallographic structure, defined as self-docking [39], was performed by using Glide Standard-Precision (SP) and it was refined with Glide Extra-Precision (XP) [40,41]. Glide has proved to be a very reliable tool for docking experiments with many successful applications in the study of protein-ligand interactions. Including *in silico* screening of novel drugs, and description of the causes of differential affinities of compounds from congeneric series [42]. The docking grid was generated with the default settings using the co-crystallized ligand in the binding site as centroid while ensuring that the grid box size was big enough to cover the entire binding site. Default docking parameters were used and the options for enhancing planarity of conjugated π groups and including aromatic carbons as H-bond donors were enabled. The same protocol was used to dock CPA into the CtpF binding site. Docking poses were visually inspected, and the pose with the best docking scores were considered. The quality of the poses were analyzed by considering RMSD values with respect to the reference coordinates (CPA in the crystallographic structure).

4.1.4 Virtual screening

The pharmacophore model was generated from the CPA-CtpF complex pose obtained in the previous molecular docking studies. The key interactions between CPA and its target were identified and defined

as a pattern for automatic searching of novel compounds fitted to this pattern. The pharmacophore-based virtual screening (PBVS) was performed using the online interface of ZINCPharmer (http://zincpharmer.csb.pitt.edu) by selecting the purchasable compounds of the ZINC database [43]. This approach included protein-ligand interactions in contact with the pharmacophore and drug-like filters [44]. The hits were also restricted to those with the best overall geometric match to the query by setting 1.0 Å as the maximum RMSD (between atomic positions of the atom of the ligand and positions of the atoms of the pattern.

The resulting candidate compounds were downloaded as a single file in sdf format, and a docking-based virtual screening (DBVS) was done on the CPA binding site of the CtpF homology model. The DBVS settings were set to the same as those used to dock CPA using Glide SP and XP. The resulting DBVS compounds were re-scored by using MM-GBSA (Molecular Mechanics combined with the Generalized-Born Surface Area) to predict more accurate binding free energies for them. MM-GBSA re-scoring allows to get a more reliable ranking. MM-GBSA implementation available in the module Prime from Schrodinger was used with the VSGB-2.0 solvation model.

4.2 Biological assays

4.2.1 Bacterial strains and growth conditions.

Mtb H37Rv, *Mtb* H37Ra, and the latter strain defective in the *ctpF* gene (*Mtb ΔctpF*) were used in this study. The mycobacterial strains were cultured in Middlebrook 7H9-OADC medium at 37 °C with agitation (180 rpm), until an OD_{590} = 0.4 for the viability assays and 0.5 for the cell membrane isolation. The *MtbΔctpF* strain was previously obtained by Milena Maya (Ph.D candidate) in our research group (unpublished results).

4.2.2 Antimicrobial susceptibility testing

The antimycobacterial activity of CPA and the compounds selected by pharmacophore-based virtual screening (PBVS) and MM-GBSA ranking were tested on *Mtb* H37Rv to determine the MIC. The purity

of the selected compounds was determined by HPLC-MS as reported by the suppliers: CPA (99.60 %; Sigma Aldrich, USA), ZINC63908257 (90.06 %; Enamine, Ukraine), ZINC55090623 (100.00 %; ChemBridge, USA), ZINC45605493 (92.70 %; Enamine, Ukraine), ZINC14541509 (99.49 %; ChemBridge, USA), ZINC09787234 (100.00 %, Enamine, Ukraine) and ZINC12584082 (98.34 %, Enamine, Ukraine). All the tested compounds were dissolved in sterile dimethyl sulfoxide (DMSO) and stored at -20 °C until use. Working compound solutions were prepared at 400 µg/mL (final concentration) in 7H9-S broth (Middlebrook 7H9 supplemented with 0.1% casitone, 0.5% glycerol, and 10% OADC [oleic acid, albumin, dextrose, and catalase]; Becton-Dickinson. The antimicrobial susceptibility assays were performed according to the recommendations of the Clinical and Laboratory Standards Institute [CLSI, formerly National Committee for Clinical Laboratory Standards (NCCLS)] with modifications [45]. Briefly, 100 µL of cultures corresponding to approximately 3.5 x 10^5 Colony Forming Units (CFU) in of Middlebrook 7H9 + OADC and tween 80 at 0.05%, pH 7.2, were separately mixed with 100 µL of serial dilutions of the compounds (from 200 to 0.78 µg/mL final concentration) in 96-well microtiter plates. The plates were incubated at 37 °C under agitation (90 rpm) for 6 days. Subsequently, 30 µL of 0.1% resazurin were added to each well, cultures were incubated for an additional 48 h at 37 °C, and viable cells were detected colorimetrically. A color change from blue to pink indicated cell growth.

The MIC corresponded to the previous concentration at which the color change was observed, corresponding to the concentration of the compound that inhibits ≥ 99% of cell growth. Cultures without bacteria (medium control), not supplemented with the compound (positive control), supplemented with rifampin 0.125 µg/mL (negative control), and with 1% DMSO (solvent control) were also assessed in triplicate as experiment controls. The cultures were performed in triplicate from three independent experiments.

The percentage of growth inhibition was determined by sub-culturing the well corresponding to the MIC for each compound in solid medium Middlebrook 7H10 supplemented with 0.1% casitone and 10% OADC; Becton-Dickinson. We determined the Colony Forming Units (CFU) after 21 days of incubation

at 37°C. The % inhibition was calculated by comparing the CFU to the 100% growth control well (without the compound).

4.2.3 Effect of CPA and selected compounds on Ca^{2+}-ATPase activity in *Mtb* plasma membrane vesicles

We assessed the effect of CPA and the selected compounds on the ATPase activity stimulated by Ca^{2+} on plasma membrane vesicles of *Mtb* H37Ra WT (*Mtb* WT) and *MtbΔctpF* cells. Mycobacterial plasma membranes were isolated using the protocol reported by Basu, with modifications [46]. The membrane protein concentration was estimated following the Bradford–Zor–Selinger method [47], using fraction V of bovine serum albumin as standard. The ATPase activity of the plasma membrane vesicles was determined by quantifying the inorganic phosphate (Pi) that was released during the P-type ATPase catalytic cycle using the Fiske-Subbarow method and bismuth citrate according to the recommendations of Cariani [48]. Briefly, the enzymatic reactions (50 µL) were carried out at pH 7.4 in incubation media (10 mM MOPS pH 7.4, 3 mM MgCl2, and 0.02% Brij-58) using 10 µg plasma membrane vesicles. The reaction buffer was supplemented with Ca^{2+} 30 µM to determine the Ca^{2+}-dependent ATPase activity. Maxchelator software (http://maxchelator.stanford.edu/) was used to calculate the Ca^{2+}-free from the total Ca^{2+} and the EGTA concentrations.

To evaluate the effect of CPA and select compounds, the reactions were individually supplemented with the compounds at 0.1 µM, 1.0 µM, 10 µM, 40 µM, 80 µM, 100 µM and 200 µM (final concentration). The maximum concentration of DMSO in the reactions was 0.5%. The reactions were pre-incubated at room temperature during 30 min; then, the enzymatic reactions were initiated by adding 3 mM Na_2ATP, incubated further for 30 min at 37 °C, and stopped by adding 100 µL of stop solution containing: 3% ascorbic acid, 0.5% ammonium molybdate, and 3% SDS in 1.0 M HCl. Finally, 150 µL of 3.5% bismuth citrate and 3.5% sodium citrate in 2.0 M HCl were added, the samples were incubated at 37 °C for 10 min, and the released inorganic phosphate (P_i) was quantified colorimetrically at 690 nm. The reactions

without protein (negative control), without Ca^{2+} (basal activity), and supplemented with the tested compounds without protein were used as controls. The Ca^{2+}-ATPase activity was calculated by the difference in ATPase activity measured in the presence and absence of calcium. Sodium orthovanadate 50 μM was used as control inhibitor of the P-type ATPase activity. In addition, the difference in Ca^{2+}-ATPase activity between the presence and absence of the compounds was considered the effect of the selected compound on the Ca^{2+}-ATPase activity. The enzymatic activity was reported as nmol of P_i released / mg protein × min, from three independent experiments. Data were analyzed using GraphPad Prism software package 5.04 (GraphPad Software, Inc). This program was also used to calculate the IC_{50}. The IC_{50} represents the drug concentration producing half-maximal inhibition of the ATPase activity. Significant differences between the ATPase activity stimulated by calcium in the presence and absence of the compounds were analyzed using the unpaired Student's t-test.

4.2.4 Cytotoxicity and hemolytic activity assays

The cytotoxic activity of CPA and the selected compounds was evaluated on murine macrophage cells of the MH-S cell line in 96-well flat-bottom plates in RPMI 1640 medium supplemented with 10% FCS. Briefly, 100 μL of the MH-S cell line (15,000 cells) were separately treated with serial dilutions of the compounds (from 200 to 0.78 μg/mL) to a final volume of 200 μL, and incubated at 37 °C and 5% CO_2 for 48 h. Subsequently, the supernatants were removed and, the cells were fixed with 100 μL of RPMI supplemented with 1% glutaraldehyde. The samples were revealed by adding 80 μL of crystal violet (CV) solution for 10 minutes. After, the wells were washed and dried for 20 minutes, and 200 μL of 10% acetic acid were added to each well to release the CV accumulated within the fixed cells [49]. The OD_{570} nm was measured using an Epoch™ 2 microplate spectrophotometer reader. MH-S cells cultures in RPMI 1640 medium supplemented with 0.25% DMSO was used as positive control. The assay was performed in triplicate from two independent experiments. Cell death > 5% was considered as a cytotoxic effect. The results were expressed as the percentage of cell death, where % viability = (OD of treated cells) / (OD of untreated cells) × 100.

The hemolytic activity assay was carried out in 96-well V-bottom plates. Briefly, 100 µL of human erythrocyte O Rh (+) suspension from healthy donors were seeded per well at 2% (final concentration) in 0.9% saline solution. The samples were then supplemented with 100 µL of serial dilutions of the compounds (from 200 to 0.78 µg/mL) and incubated at 37 °C with 5% CO_2 for 2 hours. Subsequently, the plates were centrifuged at 3500 rpm and the hemoglobin concentration was measured in the supernatants at 550 nm using an Epoch™ 2 microplate spectrophotometer reader. Cells suspended in saline solution (0% hemolysis) and distilled water (100% hemolysis) were used as negative and positive controls, respectively [50]. The experiments were performed in triplicate from two independent experiments and expressed as a percentage.

Declarations of interest

None.

Acknowledgment

This work was supported by Colciencias, Colombia [grant number 110171250419], and the Consejo Nacional de Ciencia y Tecnología (CONACyT), México (Projects Fon Inst./58/2016). Paola Santos was supported by Colciencias Ph.D, fellowship [grant number 617-2014]. David Ramírez was supported by Fondo Nacional de Desarrollo Científico y Tecnológico (FODECYT) grant 11180604 and Comisión Nacional de Investigación Científica y Tecnológica (CONICYT) REDES190074. Julio Caballero were supported by FODECYT grant 1170718.

Ethical approval

Not required

Supplementary material

Supplementary Material, Fig. S1. Alignment between 3FGO and CtpF

Alignment between: 3FGO (994 residues) and CtpF (905 residues). Program: ClustalO version 1.2.4. Progressive alignment using eight threads. Percent Identity matrix: 35.35%. Residues that are part of CPA binding pocket are shown in black boxes and the arrows represent those residues that are not

conserved.

Supplementary Material, Fig. S2. Comparison of the crystal structures of SERCA1a in complex with CPA deposited in the PDB.

A.

Crystal structures of SERCA1a in complex with CPA deposited in the PDB				
PDB code	Res	Author	Ions	Other ligands
4BEW	2.5 Å	Mattle, D.	K, Mg, Mn	ACP, ACT, MGF
3FGO	2.5 Å	Laursen, M.	K, Mg, Mn	ACP, ACT, MF4
3FPB	2.55 Å		K, Mg	ATP, MF4
3FPS	3.2 Å		Mg	ADP, MG
2EAT	2.9 Å	Takahashi, M.	-	ACE, TG1
2EAU	2.8 Å		-	ACE, PTY
4YCL	3.25 Å		K, Mg	ACE
2O9J	2.65 Å	Moncoq, K.	Na, Mg	MF4
2OA0	3.4 Å		Mg	ADP

B.

	2O9J	2OA0	3FPB	3FGO	3FPS	2EAT	4YCL	2EAU
2O9J	0.00							
2OA0	3.65	0.00						
3FPB	0.20	3.63	0.00					
3FGO	0.84	3.48	0.87	0.00				
3FPS	3.74	0.15	3.69	3.53	0.00			
2EAT	3.72	0.55	3.70	3.47	0.54	0.00		
4YCL	3.68	0.50	3.73	3.66	0.48	0.52	0.00	
2EAU	3.98	0.66	4.02	4.11	0.72	0.78	0.73	0.00

C.

Glu 56 / 63		Leu 61 / 68		Asn 101 / 98		Ala 102 / 99		Phe 256 / 248		Pro 312 / 294	
	CtpF		CtpF		CtpF		CtpF		CtpF		CtpF
CtpF	0.00	CtpF	0.00	CtpF	0.00	CtpF	0.00	CtpF	0.00	CtpF	0.00
2O9J	0.88	2O9J	2.58	2O9J	4.31	2O9J	4.77	2O9J	3.60	2O9J	3.92
2OA0	2.29	2OA0	1.23	2OA0	3.24	2OA0	3.54	2OA0	3.87	2OA0	3.52
3FPB	3.57	3FPB	2.47	3FPB	4.14	3FPB	5.14	3FPB	3.57	3FPB	3.63
3FGO	0.36	3FGO	1.39	3FGO	0.65	3FGO	0.11	3FGO	1.89	3FGO	1.99
3FPS	0.69	3FPS	1.31	3FPS	2.91	3FPS	3.36	3FPS	3.77	3FPS	3.41
2EAT	2.19	2EAT	0.98	2EAT	3.63	2EAT	3.22	2EAT	4.36	2EAT	3.47
4YCL	1.44	4YCL	1.81	4YCL	3.27	4YCL	3.45	4YCL	3.63	4YCL	3.28
2EAU	3.06	2EAU	2.12	2EAU	2.92	2EAU	4.29	2EAU	3.21	2EAU	3.15

Comparison of the 3D structures of SERCA1a in complex with CPA. A. Summary table of all the SERCA1a-CPA complex structures registered in PDB (https://www.rcsb.org). B. Comparison matrix of all the crystallized structures. C. Comparison matrix of the binding site residues with CPA. The smaller RMSDs are represented in green. The alignment, RMSD and score are computed from the C-alpha atoms of the aligned residues.

References

1. World Health Organization. *Global Tuberculosis Report 2019*.; 2019. doi:ISBN 978 92 4

156539 4

2. Dheda K, Gumbo T, Maartens G, et al. The epidemiology, pathogenesis, transmission, diagnosis, and management of multidrug-resistant, extensively drug-resistant, and incurable tuberculosis. *Lancet Respir Med*. 2017. doi:10.1016/S2213-2600(17)30079-6

3. Yatime L, Buch-Pedersen MJ, Musgaard M, et al. P-type ATPases as drug targets: Tools for medicine and science. *Biochim Biophys Acta - Bioenerg*. 2009;1787(4):207-220. doi:10.1016/j.bbabio.2008.12.019

4. Dupont C, Viljoen A, Thomas S, et al. Bedaquiline inhibits the ATP synthase in mycobacterium abscessus and is effective in infected zebrafish. *Antimicrob Agents Chemother*. 2017;61(11):1. doi:10.1128/AAC.01225-17

5. Vasava MS, Bhoi MN, Rathwa SK, Borad MA, Nair SG, Patel HD. Drug development against tuberculosis: Past, present and future. *Indian J Tuberc*. 2017;64(4):252-275. doi:10.1016/j.ijtb.2017.03.002

6. Raimunda D, Long JE, Padilla-benavides T, et al. Differential roles for the Co2+/Ni2+ transporting ATPases, CtpD and CtpJ, in Mycobacterium tuberculosis virulence. *Mol Microbiol*. 2014;91(1):185-197. doi:10.1111/mmi.12454

7. Krishna S, Pulcini S, Fatih F, Staines H. Artemisinins and the biological basis for the PfATP6/SERCA hypothesis. *Trends Parasitol*. 2010;26(11):517-523. doi:10.1016/j.pt.2010.06.014

8. Palmgren MG, Nissen P. P-Type ATPases. *Annu Rev Biophys*. 2011;40(1):243-266. doi:10.1146/annurev.biophys.093008.131331

9. Bublitz M, Morth JP, Nissen P. P-type ATPases at a glance. *J Cell Sci*. 2012;124:2515-2519.

doi:10.1242/jcs.102921

10. Novoa-Aponte L, León-Torres A, Patiño-Ruiz M, et al. In silico identification and characterization of the ion transport specificity for P-type ATPases in the Mycobacterium tuberculosis complex. *BMC Struct Biol*. 2012;12:25. doi:10.1186/1472-6807-12-25

11. Ward SK, Abomoelak B, Hoye EA, Steinberg H, Talaat AM. CtpV: A putative copper exporter required for full virulence of Mycobacterium tuberculosis. *Mol Microbiol*. 2010;77(5):1096-1110. doi:10.1111/j.1365-2958.2010.07273.x

12. Padilla-Benavides T, Long JE, Raimunda D, Sassetti CM, Argüello JM. A novel P(1B)-type Mn2+-transporting ATPase is required for secreted protein metallation in mycobacteria. *J Biol Chem*. 2013;288(16):11334-11347. doi:10.1074/jbc.M112.448175

13. Pulido PA, Novoa-Aponte L, Villamil N, Soto CY. The DosR Dormancy Regulator of Mycobacterium tuberculosis Stimulates the Na(+)/K (+) and Ca (2+) ATPase Activities in Plasma Membrane Vesicles of Mycobacteria. *Curr Microbiol*. 2014;69(5):604-610. doi:10.1007/s00284-014-0632-6

14. Novoa-Aponte L, Soto Ospina CY. Mycobacterium tuberculosis P-type ATPases: Possible Targets for Drug or Vaccine Development. *Biomed Res Int*. 2014;2014:296. doi:10.1155/2014/296986

15. Chourasia M, Sastry GN. The Nucleotide, Inhibitor, and Cation Binding Sites of P-type II ATPases. *Chem Biol Drug Des*. 2012;79(5):617-627. doi:10.1111/j.1747-0285.2012.01334.x

16. Martinez-Azorin F. Cyclopiazonic acid reduces the coupling factor of the Ca2+-ATPase acting on Ca2+ binding. *FEBS Lett*. 2004;576(1):73-76. doi:10.1016/j.febslet.2004.08.064

17. Novoa-Aponte L, León-Torres A, Patiño-Ruiz M, et al. In silico identification and

characterization of the ion transport specificity for P-type ATPases in the Mycobacterium tuberculosis complex. *BMC Struct Biol*. 2012;12:25. doi:10.1186/1472-6807-12-25

18. Sievers F, Higgins DG. Clustal Omega. *Curr Protoc Bioinforma*. 2014. doi:10.1002/0471250953.bi0313s48

19. Laursen M, Bublitz M, Moncoq K, et al. Cyclopiazonic acid is complexed to a divalent metal ion when bound to the sarcoplasmic reticulum Ca2+-ATPase. *J Biol Chem*. 2009;284(20):13513-13518. doi:10.1074/jbc.C900031200

20. Moncoq K, Trieber C a, Young HS. The molecular basis for cyclopiazonic acid inhibition of the sarcoplasmic reticulum calcium pump. *J Biol Chem*. 2007;282(13):9748-9757. doi:10.1074/jbc.M611653200

21. Gilson MK, Zhou H-X. Calculation of Protein-Ligand Binding Affinities. *Annu Rev Biophys Biomol Struct*. 2007;36(1):21-42. doi:10.1146/annurev.biophys.36.040306.132550

22. Aparna V, Dineshkumar K, Mohanalakshmi N, Velmurugan D, Hopper W. Identification of natural compound inhibitors for multidrug efflux pumps of Escherichia coli and Pseudomonas aeruginosa using in silico high-throughput virtual screening and in vitro validation. *PLoS One*. 2014;9(7). doi:10.1371/journal.pone.0101840

23. Santos P, López-Vallejo F, Soto CY. In silico approaches and chemical space of anti-P-type ATPase compounds for discovering new antituberculous drugs. *Chem Biol Drug Des*. 2017;90(2):175-187. doi:10.1111/cbdd.12950

24. Hymery N, Masson F, Barbier G, Coton E. Cytotoxicity and immunotoxicity of cyclopiazonic acid on human cells. *Toxicol Vitr*. 2014;28(5):940-947. doi:10.1016/j.tiv.2014.04.003

25. Yao S, Gallenkamp D, Wölfel K, Lüke B, Schindler M, Scherkenbeck J. Synthesis and SERCA

activities of structurally simplified cyclopiazonic acid analogues. *Bioorganic Med Chem*. 2011;19(15):4669-4678. doi:10.1016/j.bmc.2011.06.001

26. Saffioti NA, de Sautu M, Ferreira-Gomes MS, et al. E2P-like states of plasma membrane Ca2+-ATPase characterization of vanadate and fluoride-stabilized phosphoenzyme analogues. *Biochim Biophys Acta - Biomembr*. 2019;1861(2):366-379. doi:10.1016/j.bbamem.2018.11.001

27. Di Marino D, D'Annessa I, Coletta A, Via A, Tramontano A. Characterization of the differences in the cyclopiazonic acid binding mode to mammalian and P. Falciparum Ca2+ pumps: A computational study. *Proteins Struct Funct Bioinforma*. 2015;83(3):564-574. doi:10.1002/prot.24734

28. Kotšubei A, Gorgel M, Morth JP, Nissen P, Andersen JL. Probing determinants of cyclopiazonic acid sensitivity of bacterial Ca 2+-ATPases. In: *FEBS Journal*. Vol 280. ; 2013:5441-5449. doi:10.1111/febs.12310

29. Rosch JW, Sublett J, Gao G, Wang YD, Tuomanen EI. Calcium efflux is essential for bacterial survival in the eukaryotic host. *Mol Microbiol*. 2008;70(2):435-444. doi:10.1111/j.1365-2958.2008.06425.x

30. Cui R, Wang Y, Wang L, et al. Cyclopiazonic acid, an inhibitor of calcium-dependent ATPases with antiviral activity against human respiratory syncytial virus. *Antiviral Res*. 2016;132:38-45. doi:10.1016/j.antiviral.2016.05.010

31. Krishna S, Pulcini S, Moore CM, Teo BHY, Staines HM. Pumped up: Reflections on PfATP6 as the target for artemisinins. *Trends Pharmacol Sci*. 2014;35(1):4-11. doi:10.1016/j.tips.2013.10.007

32. Naik PK, Srivastava M, Bajaj P, et al. The binding modes and binding affinities of artemisinin

derivatives with Plasmodium falciparum Ca2+-ATPase (PfATP6). *J Mol Model*. 2011;17(2):333-357. doi:10.1007/s00894-010-0726-4

33. Biasini M, Bienert S, Waterhouse A, et al. SWISS-MODEL: Modelling protein tertiary and quaternary structure using evolutionary information. *Nucleic Acids Res*. 2014;42(W1):252-258. doi:10.1093/nar/gku340

34. Bowers KJ, Sacerdoti FD, Salmon JK, et al. Molecular dynamics---Scalable algorithms for molecular dynamics simulations on commodity clusters. In: *Proceedings of the 2006 ACM/IEEE Conference on Supercomputing - SC '06*. ; 2006:84. doi:10.1145/1188455.1188544

35. Wiederstein M, Sippl MJ. ProSA-web: interactive web service for the recognition of errors in three-dimensional structures of proteins. *Nucleic Acids Res*. 2007;35(SUPPL.2):W407-10. doi:10.1093/nar/gkm290

36. Laskowski RA, MacArthur MW, Moss DS, Thornton JM. PROCHECK: a program to check the stereochemical quality of protein structures. *J Appl Crystallogr*. 1993;26(2):283-291. doi:10.1107/S0021889892009944

37. Sterling T, Irwin JJ. ZINC 15 - Ligand Discovery for Everyone. *J Chem Inf Model*. 2015;55(11):2324-2337. doi:10.1021/acs.jcim.5b00559

38. MacroModel, Schrödinger, LLC, New York, NY 2016. MacroModel. 2016. www.schrodinger.com.

39. Ramírez D, Caballero J. Is it reliable to take the molecular docking top scoring position as the best solution without considering available structural data? *Molecules*. 2018;23(5). doi:10.3390/molecules23051038

40. Friesner RA, Banks JL, Murphy RB, et al. Glide: a new approach for rapid, accurate docking

and scoring. Method and assessment of docking accuracy. *J Med Chem*. 2004;47(7):1739-1749. doi:10.1021/jm0306430

41. Friesner RA, Murphy RB, Repasky MP, et al. Extra precision glide: Docking and scoring incorporating a model of hydrophobic enclosure for protein-ligand complexes. *J Med Chem*. 2006. doi:10.1021/jm051256o

42. Mena-Ulecia K, Tiznado W, Caballero J. Study of the differential activity of thrombin inhibitors using docking, QSAR, molecular dynamics, and MM-GBSA. *PLoS One*. 2015. doi:10.1371/journal.pone.0142774

43. Wolber G, Langer T. LigandScout: 3-D pharmacophores derived from protein-bound ligands and their use as virtual screening filters. *J Chem Inf Model*. 2005;45(1):160-169. doi:10.1021/ci049885e

44. Veber DF, Johnson SR, Cheng HY, Smith BR, Ward KW, Kopple KD. Molecular properties that influence the oral bioavailability of drug candidates. *J Med Chem*. 2002;45(12):2615-2623. doi:10.1021/jm020017n

45. Martin A, Camacho M, Portaels F, Palomino JC. Resazurin Microtiter Assay Plate Testing of Mycobacterium tuberculosis Susceptibilities to Second-Line Drugs: Rapid, Simple, and Inexpensive Method. *Antimicrob Agents Chemother*. 2003;47(11):3616-3619. doi:10.1128/AAC.47.11.3616-3619.2003

46. Santos P, Gordillo A, Osses L, Salazar LM, Soto CY. Effect of antimicrobial peptides on ATPase activity and proton pumping in plasma membrane vesicles obtained from mycobacteria. *Peptides*. 2012;36(1):121-128. doi:10.1016/j.peptides.2012.04.018

47. Zor T, Selinger Z. Linearization of the Bradford protein assay increases its sensitivity:

Theoretical and experimental studies. *Anal Biochem*. 1996;236(2):302-308. doi:10.1006/abio.1996.0171

48. León-Torres A, Novoa-Aponte L, Soto C-Y. CtpA, a putative Mycobacterium tuberculosis P-type ATPase, is stimulated by copper (I) in the mycobacterial plasma membrane. *BioMetals*. 2015;28(4):713-724. doi:10.1007/s10534-015-9860-x

49. Ishiyama M, Tominaga H, Shiga M, SASAMOTO K, OHKURA Y, UENO K. A combined assay of cell viability and in vitro cytotoxicity with a highly water-soluble tetrazolium salt, neutral red and crystal violet. *Biol Pharm Bull*. 1996;19(11):1518-1520. doi:10.1248/bpb.19.1518

50. Braga AA, e Lacerda RR, de Vasconcelos Medeiros GKV, et al. Antibacterial and Hemolytic Activity of a new Lectin Purified from the Seeds of Sterculia Foetida L. *Appl Biochem Biotechnol*. 2014;175(3):1689-1699. doi:10.1007/s12010-014-1390-4

Graphical abstract